Journal of Materials Chemistry B

PAPER

View Article Online
View Journal | View Issue

Cite this: J. Mater. Chem. B, 2014, 2, 502

Water-soluble copolymeric materials: switchable NIR two-photon fluorescence imaging agents for living cancer cells†

Nan Xie,[a] Ke Feng,*[b] Bin Chen,[b] Ming Zhao,[a] Shiqi Peng,*[a] Li-Ping Zhang,[b] Chen-Ho Tung[b] and Li-Zhu Wu*[b]

Received 10th September 2013
Accepted 26th October 2013

DOI: 10.1039/c3tb21251c

www.rsc.org/MaterialsB

A simple one-pot multi-component ROMP of hydrophilic, spiropyran (SP) and *tert*-butyloxycarbonyl-protected (Boc-protected) amino-functionalized norbornenes was developed, and a series of water-soluble copolymeric materials were provided. The photochromic SP moiety endows the copolymers the properties of switchable fluorescence imaging with alternating near-IR (NIR) two-photon and visible single-photon excitations; thereby the copolymers can serve as a promising NIR two-photon fluorescent probe for living cancer cells. The cationic ammonium group enhances the cell transporting capability of the copolymers as well. The present strategy of one-pot ROMP also makes polynorbornene a modular and flexible scaffold in designing and synthesizing specifically biocompatible polymers with applications in imaging, diagnosis and therapy.

Introduction

Fluorescence imaging is one of the indispensable tools for highly-sensitive and non-invasive visualization, characterization and quantification of normal or pathological processes in cells, tissues and living organisms.[1–5] To support the required needs for imaging, as well as diagnosis and therapy, there has been considerable interest in investigating highly specific targeting and labelling materials such as small organic dyes,[6–8] inorganic nanoparticles,[9–16] liposome assemblies and polymers.[17–20] Far from the undesirable leakage of small organic dyes or the unexpected aggregation of inorganic nanoparticles, polymeric fluorescent materials have attracted increasing attention due to their uniform characteristics in component, structure, stability, assembly in biological environment and the convenience for multipurpose design and synthesis.[17–20] On one hand, polymers can easily integrate more than one component with multimodal imaging and functionality; on the other hand, the multivalent effect[21] and enhanced permeation and retention effect,[22–24] attributed to the repeat units on the polymer chain, can greatly increase the signal-to-noise ratio for higher imaging quality and target-binding specificity.

To date, polymeric imaging materials have been achieved primarily by two types of strategies, amphiphilic block copolymers[19,25,26] and conjugated electrolytes.[27–29] Multi-functional groups can be tethered on polymer backbones through chemical modification step-by-step, however, neither of these strategies avoid tedious and time-consuming multi-step copolymerization (even coupled with varied polymerization methods) or post-polymerization treatment. Different from these strategies, random copolymers can be constructed with diverse components in a single polymerization step and afford biocompatible imaging materials,[30–32] but a series of problems, such as functional monomer synthesis, stability of the monomers, tolerance of the initiators and the control of the polymeric molecular weights and polydispersity indices (PDIs) and yields, remain to be solved.

Ring-opening metathesis polymerization (ROMP) is a powerful toolkit for the preparation of random, block and alternating functionalized copolymers.[33–57] Using ruthenium *N*-heterocyclic carbene complexes as initiators, controlled polymer backbones, such as polynorbornenes, have been obtained from varied function monomers containing chromophores, hydrophilic tails and hydrogen-bond interfaces, oligopeptides, ionic and/or metallic compounds.[40–57]

Previously, we reported a simple one-pot ROMP using functionalized norbornenes to prepare random copolymers in water.[58] This strategy allows hydrophobic fluorescence chromophores through multi-component copolymerization to be conveniently introduced into an aqueous medium. On this basis, we synthesized water-soluble imaging random

[a]School of Chemical Biology and Pharmaceutical Sciences, Capital Medical University, Beijing 100069, P. R. China. E-mail: sqpeng@bjmu.edu.cn; Fax: +86 10 8391 1528; Tel: +86 10 8391 1528

[b]Key Laboratory of Photochemical Conversion and Optoelectronic Materials, Technical Institute of Physics and Chemistry, Chinese Academy of Sciences, Beijing 100190, P. R. China. E-mail: kefeng@mail.ipc.ac.cn; lzwu@mail.ipc.ac.cn; Fax: +86 10 8254 3580; Tel: +86 10 8254 3580

† Electronic supplementary information (ESI) available: GPC curves, NMR, mass spectra, decay profiles and fluorescent images for the intermediates, monomers and polymers. See DOI: 10.1039/c3tb21251c

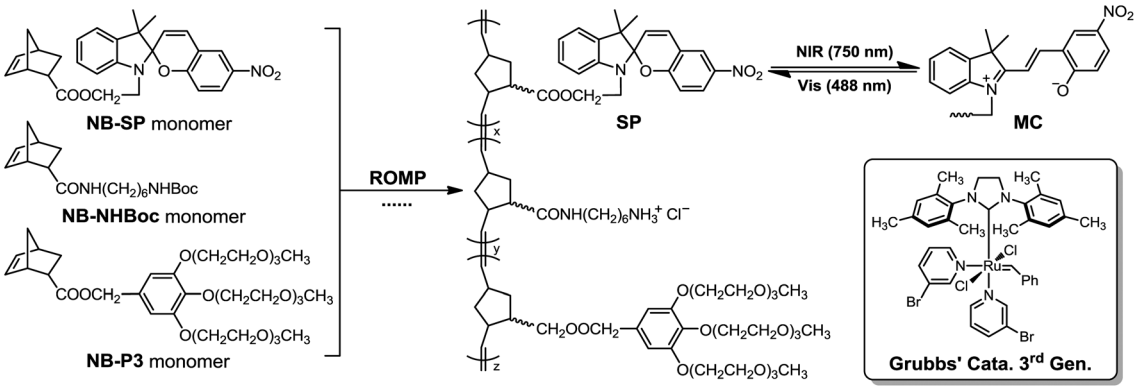

Scheme 1 The preparation of PNB–SP_x-*co*-$(NH_2 \cdot HCl)_y$-*co*-$P3_z$ water-soluble random copolymers.

copolymers PNB–SP_x-*co*-$(NH_2 \cdot HCl)_y$-*co*-$P3_z$ in the present work (Scheme 1). We selected spiropyran as the fluorescence chromophore for the photochromic possession of a nonfluorescent spiropyran (SP) form and a highly fluorescent merocyanine (MC) form, as well as the reported two-photon fluorescence,[59–62] which has the potential to cause less photo-induced damage and phototoxicity, a low autofluorescence background, better spatial localization and deeper tissue penetration.[63–68] As we expected, the polymers exhibited switchable fluorescence imaging characteristics with alternating NIR two-photon and visible single-photon excitations in living cancer cells, such as Bel-7402, HepG2, MCF-7 and A549. Furthermore, a cationic ammonium group was introduced to enhance the cell transporting capability[69] of the copolymers through a standard treatment of the Boc-protected amino group. Importantly, such a one-pot ROMP strategy will make polynorbornene a modular and flexible scaffold to design and synthesize specific biocompatible polymers for multipurpose applications in imaging, diagnosis and therapy.

Experimental section

General

All of the experiments with air- and moisture-sensitive intermediates and compounds were carried out under an inert atmosphere using standard Schlenk techniques. NMR spectra were recorded on a Bruker Advance DPX 400 MHz spectrometer and referenced using the residual proton signal of the solvent. Mass spectra were obtained on either a Bruker APEX II or a Bruker BIFLEX III spectrometer. Elemental analyses were performed on a Carlo Erba 1106 elemental analyzer. FT-IR spectra were taken on an Excalibur 3100 system (varian, USA). UV-Vis spectra were obtained using a Shimadzu 1601PC spectrophotometer. Fluorescence measurements were run on an F-900 Edinburgh Analytical Instruments spectrometer. Gel-permeation chromatography (GPC) analyses were carried out on a multi-angle, digital signal processing light scattering system (Wyatt, USA) using a Shimadzu LC-10A pump coupled to a Dawn Heleos II light scattering detector (equipped with a 100 mW GaAs laser) and a Optilab rEX interferometeric refractometer with THF or DMF (with 10 mM LiBr at 313 K) as eluents on a 10 μm linear MZ-Gel SDplus column. The flow rate used for all of the measurements was 0.5 mL min^{-1}. No calibration standards were used, and d*n*/d*c* values were obtained for each injection by assuming 100% mass elution from the columns. M_w, M_n and PDIs were calculated using an Astra 5 software package. Commercially available LEDs were employed as UV (365 nm, input 350 mA, 3.7 V, output ~125 mW cm^{-2}) and visible (530 nm, input 350 mA, 3.4 V, output ~120 mW cm^{-2}) light sources, and the intensities were determined by a Newport (CA, USA) Optical Power/Energy Meter Model 842-PE instrument. Zeta potential measurements were performed in 10 mM PBS buffer with a pH value of 7.4 at 298 K, using a Nano-2S90 Zetasizer (Malvern, UK). The zeta potential (ζ) was calculated from the electrophoretic mobility using the Smoluchowski equation as the average values of three runs.

Materials and synthesis

Exo-bicyclo[2.2.1]hept-5-ene-2-carboxylic acid was synthesized according to published procedures.[70–72] Dulbecco's modified Eagle's medium (DMEM), RPMI 1640 medium and fetal bovine serum (FBS) were purchased from Gibco. 3-(4,5-Dimethylthiazol-2-yl)-2,5-diphenyltetrazolium bromide (MTT), penicillin, streptomycin and 4% paraformaldehyde solution in PBS were purchased from Beijing Solarbio Science & Technology Co. Ltd. The other reagents and solvents were obtained from commercial supplies and used as received without further purification.

***N*-*tert*-Butoxycarbonyl-1,6-diaminohexyl-*exo*-bicyclo[2.2.1]-hept-5-ene-2-carboxamide (NB–Boc–NH monomer).** *N*-(*tert*-Butoxycarbonyl)hexyl diamine was synthesized analogously to the literature.[73] At 0 °C, to a solution of 1,6-diaminohexane (11.70 g, 101 mmol) in methylene chloride (100 mL), a solution of Boc anhydride (4.40 g, 20.2 mmol, 30 mL in CH_2Cl_2) was added dropwise. Then the mixture was stirred at 0 °C for 30 min, and at room temperature overnight. The unreacted 1,6-diaminohexane was removed under vacuum conditions at 85 °C, and the residue was washed with saturated Na_2CO_3 solution and dried over $NaSO_4$ to afford *N*-(*tert*-butoxycarbonyl)-hexyl diamine (4.20 g, 19.4 mmol, yield 96%) as a transparent oil, and used for the next reaction without further purification. ^1H NMR (400 MHz, $CDCl_3$) δ: 4.70 (br, 1H), 3.02 (m, 2H), 2.62 (m, 2H), 1.37 (s, 15H), 1.26 (m, 4H).

A mixture of *N*-(*tert*-butoxycarbonyl)hexyl diamine (1.10 g, 5.09 mmol), *exo*-bicyclo[2.2.1]hept-5-ene-2-carboxylic acid (0.70 g, 5.07 mmol), PyBOP (benzotriazole-1-yl-oxytripyrrolidinophosphonium hexafluorophosphate, 3.20 g, 6.15 mmol) and TEA (triethylamine, 1 mL) was stirred in anhydrous DMF (20 mL) under an inert atmosphere for 1 h. After removal of the solvent, the crude product was purified by silica gel column chromatography to give the NB–Boc–NH monomer as a colorless powder (1.55 g, 4.61 mmol, yield 91%). TLC: R_f = 0.30 (methylene chloride : ethyl acetate = 4 : 1). ESI-MS: m/z = 359 $[M + Na]^+$, 375 $[M + K]^+$. ^{1}H NMR (400 MHz, $CDCl_3$) δ: 6.06 (m, 2H), 5.85 (br, 1H), 4.63 (br, 1H), 3.20 (m, 2H), 3.06 (m, 2H), 2.87 (m, 2H), 1.96 (m, 1H), 1.86 (m, 1H), 1.69 (m, 1H), 1.45 (m, 4H), 1.40 (s, 9H), 1.30 (m, 6H). $^{13}C\{^1H\}$ NMR (100 MHz, $CDCl_3$) δ: 175.55, 156.01, 138.07, 135.98, 78.92, 47.15, 46.24, 44.53, 41.47, 40.11, 39.15, 30.40, 29.92, 29.51, 28.34, 26.18, 26.04. Anal. calcd for $C_{19}H_{32}N_2O_3$: C, 67.82; H, 9.59; N, 8.33. Found: C, 67.91; H, 9.39; N, 8.56%. FT-IR (KBr): ν = 3460, 3333, 3060, 2976, 2934, 2864, 1689, 1649, 1539, 1478, 1453, 1442, 1388, 1365, 1333, 1276, 1253, 1178, 1050, 1021, 870, 781, 760, 732 cm^{-1}.

2-(3′,3′-Dimethyl-6-nitro-3′*h*-spiro[chromene-2,2′-indo]-1′-yl)-ethyl-*exo*-bicyclo[2.2.1]-hept-5-ene-2-carboxylate (NB–SP monomer). The NB–SP monomer was synthesized according to our previous reports.[58,74] EI-MS: m/z = 472 $[M]^+$. ^{1}H NMR (400 MHz, $CDCl_3$, ppm) δ: 8.01 (m, 2H), 7.21 (t, 1H, J = 10.6 Hz), 7.09 (d, 1H, J = 7.2 Hz), 6.91 (m, 2H), 6.72 (m, 2H), 6.13 (m, 1H), 6.07 (m, 1H), 5.89 (d, 1H, J = 10.4 Hz), 4.29 (m, 1H), 4.21 (m, 1H), 3.53 (m, 1H), 3.43 (m, 1H), 2.92 (m, 1H), 2.90 (s, 1H), 2.14 (m, 1H), 1.86 (m, 1H), 1.46 (m, 1H), 1.34 (m, 2H), 1.29 (m, 3H), 1.18 (m, 3H). $^{13}C\{^1H\}$ NMR (100 MHz, $CDCl_3$, ppm) δ: 176.06, 159.36, 146.64, 141.01, 138.06, 138.01, 135.59, 135.54, 128.24, 127.77, 125.89, 122.70, 121.75, 119.84, 118.39, 115.49, 106.74, 106.45, 62.36, 52.79, 46.49 & 46.41 (*isomers*), 46.28, 42.99 & 42.96 (*isomers*), 42.40, 41.53, 30.38 & 30.34 (*isomers*), 25.80, 19.80. Anal. calcd for $C_{28}H_{28}N_2O_5$: C, 71.17; H, 5.97; N, 5.93. Found: C, 70.82; H, 5.95; N, 5.87%. FT-IR (KBr): ν = 3420, 3279, 3062, 2967, 2933, 2868, 2855, 1725, 1653, 1612, 1512, 1483, 1458, 1445, 1383, 1363, 1337, 1298, 1275, 1170, 1091, 1049, 1029, 955, 921, 810, 750, 720, 683 cm^{-1}.

3,4,5-Tris-(1,4,7,10-tetraoxaundecyl)benzyl-*exo*-bicyclo[2.2. 1]-hept-5-ene-2-carboxylate (NB–P3 monomer). The NB–P3 monomer was synthesized according to our previous report.[58] EI-MS: m/z = 714 $[M]^+$. ^{1}H NMR (400 MHz, $CDCl_3$, ppm) δ: 6.57 (s, 2H), 6.10 (m, 2H), 4.99 (s, 2H), 4.14 (t, 6H, J = 4.6 Hz), 3.83 (m, 4H), 3.77 (m, 2H), 3.70 (m, 6H), 3.63 (m, 12H), 3.52 (m, 6H), 3.35 (s, 9H), 3.04 (m, 1H), 2.91 (m, 1H), 2.25 (m, 1H), 1.91 (m, 1H), 1.50 (m, 1H), 1.36 (m, 2H). $^{13}C\{^1H\}$ NMR (100 MHz, $CDCl_3$, ppm) δ: 175.49, 152.30, 137.99, 137.69, 135.31, 131.24, 107.49, 71.91, 71.55, 70.43, 70.30, 70.14, 69.33, 68.53, 65.83, 58.58, 46.24, 45.95, 42.74, 41.25, 30.02. Anal. calcd for $C_{36}H_{58}O_{14}$: C, 60.49; H, 8.18. Found: C, 60.65; H, 8.13%. FT-IR (KBr): ν = 3062, 2975, 2930, 2875, 2820, 1728, 1592, 1504, 1456, 1439, 1367, 1349, 1334, 1247, 1233, 1200, 1111, 1026, 942, 852, 723, 702 cm^{-1}.

General polymerization and deprotection procedure

A solution of Grubbs' third-generation initiator[37] (~0.01 M) was added to a methylene chloride solution (~0.05 M) containing the spiropyran monomer NB–SP, NB–P3 monomer and NB–Boc–NH monomer in varied ratios. The reaction mixture was stirred for 15 min at room temperature. After complete conversion of the monomer (>99%, monitored by ^{1}H NMR), the polymerization was quenched by the addition of ethyl vinyl ether and stirred for an additional 15 min. The polymer was precipitated with cold ether, and dried at room temperature under high vacuum.

Polymer PNB–Boc–NH. ^{1}H NMR (400 MHz, $CDCl_3$, ppm) δ: 5.78 (br, 1H), 5.27 (m, 2H), 4.90 (br, 1H), 3.15 (m, 2H), 3.05 (m, 4H), 2.64 (m, 1H), 2.28 (m, 1H), 2.14 (m, 1H), 1.90 (m, 1H), 1.56 (m, 1H), 1.41 (m, 12H), 1.28 (br, 4H), 1.10 (br, 1H). FT-IR (KBr): ν = 3462, 3332, 3060, 2977, 2933, 2864, 1689, 1646, 1538, 1479, 1454, 1441, 1387, 1365, 1333, 1275, 1252, 1176, 1048, 1020, 869, 782, 762, 731 cm^{-1}.

Polymer PNB–SP. ^{1}H NMR (400 MHz, $CDCl_3$, ppm) δ: 7.96 (br, 2H), 7.14 (br, 1H), 7.05 (br, 1H), 6.86 (br, 2H), 6.66 (br, 2H), 5.83 (br, 1H), 5.27 (br, 2H), 4.16 (br, 2H), 3.37 (br, 2H), 2.92 (br, 1H), 2.57 (br, 1H), 1.92 (br, 2H), 1.60 (br, 1H), 1.26 (br, 5H), 1.12 (br, 3H). FT-IR (KBr): ν = 3421, 3281, 3062, 2968, 2932, 2868, 2855, 1725, 1654, 1611, 1512, 1483, 1458, 1446, 1382, 1362, 1337, 1297, 1275, 1170, 1091, 1049, 1028, 955, 920, 810, 750, 719, 683 cm^{-1}.

Polymer PNB–P3. ^{1}H NMR (400 MHz, $CDCl_3$, ppm) δ: 6.53 (br, 2H), 5.35 (m, 2H), 4.88 (br, 2H), 4.10 (br, 6H), 3.81 (m, 4H), 3.76 (m, 2H), 3.69 (m, 6H), 3.63 (m, 12H), 3.52 (m, 6H), 3.34 (br, 9H), 3.10 (m, 1H), 2.75 (m, 1H), 2.53 (br, 1H), 2.03 (br, 2H), 1.66 (br, 1H), 1.13 (br, 1H). FT-IR (KBr): ν = 3059, 2974, 2928, 2875, 2817, 1728, 1591, 1505, 1455, 1439, 1366, 1349, 1333, 1248, 1234, 1199, 1112, 1027, 942, 853, 724, 702 cm^{-1}.

Copolymer PNB–SP_{20}-*co*-$(Boc–NH)_{20}$-*co*-$P3_{60}$. ^{1}H NMR (400 MHz, $CDCl_3$, ppm) δ: 7.96 (br, 0.4H), 7.13 (br, 0.2H), 7.04 (br, 0.2H), 6.85 (br, 0.4H), 6.72 (br, 0.4H), 6.66 (br, 1.2H), 5.89 (br, 0.2H), 5.20 (m, 2H), 4.94 (m, 1.4H), 4.10 (m, 4H), 3.81 (m, 2.4H), 3.76 (m, 1.2H), 3.69 (m, 3.6H), 3.63 (m, 7.2H), 3.52 (m, 3.6H), 3.34 (m, 5.8H), 2.99 (m, 2H), 2.54 (m, 1.6H), 2.05 (m, 1.8H), 1.72 (m, 1H), 1.43 (m, 5.6H). FT-IR (KBr): ν = 3470, 3369, 3248, 3059, 2932, 2872, 2819, 1729, 1711, 1650, 1632, 1608, 1594, 1544, 1520, 1509, 1483, 1458, 1440, 1384, 1364, 1350, 1337, 1298, 1273, 1250, 1199, 1167, 1112, 1092, 1043, 1028, 954, 851, 810, 749 cm^{-1}.

The copolymers were deprotected in a mixture of 95% TFA, 2.5% H_2O and 2.5% triisopropylsilane for 20 min, then precipitated in cold ether. The crude products were collected by centrifugation and purified by dialysis (Spectra/Por 1 membrane, MWCO 6000–8000) against water for 5 days at 4 °C. After lyophilisation, the resulting copolymers were obtained as yellow solids.

Copolymer PNB–SP_{20}-*co*-$(NH_2 \cdot HCl)_{20}$-*co*-$P3_{60}$. ^{1}H NMR (400 MHz, DMSO-d_6/$CDCl_3$ (v/v, 3 : 1), ppm) δ: 7.99 (br, 0.4H), 6.98 (m, 0.4H), 6.68 (br, 0.4H), 6.49 (br, 1.6H), 5.83 (br, 0.2H), 5.13 (m, 2H), 4.87 (m, 1.4H), 4.01 (m, 4H), 3.72 (m, 2.4H), 3.66 (m, 1.2H), 3.59 (m, 3.6H), 3.52 (m, 7.2H), 3.41 (m, 3.6H), 3.23 (m, 5.8H), 3.00 (m, 2H), 2.76 (m, 1.2H), 2.32 (m, 0.4H), 1.89 (m, 1.8H), 1.60 (m, 1H), 1.23 (m, 3.8H). FT-IR (KBr): ν = 3413, 3252, 3051, 2935, 2871, 2820, 1730, 1649, 1607, 1592, 1546, 1518, 1509, 1487, 1457, 1440, 1381, 1363, 1350, 1332, 1298, 1249, 1199, 1162, 1111, 1090, 1027, 952, 851, 811, 749 cm^{-1}.

Cell culture

Human breast adenocarcinoma (MCF-7) cells, human hepatoma (Bel-7402) cells and human lung adenocarcinoma cells (A549) were cultured in RPMI 1640 medium, and human liver carcinoma (HepG2) cells were cultured in Dulbecco's Modified Eagle Medium (DMEM). Both of the media contained 10% fetal bovine serum (FBS), 100 mg L^{-1} streptomycin and 100 U mL^{-1} penicillin. The cells were maintained in a humidified atmosphere of 5% CO_2 at 37 °C.

Cytotoxicity assay

The cytotoxicity studies were measured using the 3-(4,5-dimethylthiazol-2-yl)-2,5-diphenyltetrazolium bromide (MTT) assay. Cells growing in the log phase were seeded into 96-well cell-culture plates at a density of 5×10^4 per well, and incubated overnight in 5% CO_2 at 37 °C. The polymeric probes were added to the wells of the treatment group at concentrations of 0.00625, 0.0125, 0.025, 0.050, 0.10 and 0.20 mg mL^{-1}. The cells were incubated for 24 h, and then 5 mg mL^{-1} MTT (25 μL per well) in PBS solution was added to each well. After incubation for an additional 4 hours, the formazan crystals generated by dehydrogenases in live cells were dissolved in DMSO and the absorbance was recorded at 492 nm by using a microplate reader (Multiskan MK3, Thermo Electron Corporation). The viability of the cells can be calculated as the ratio of the mean absorbance for the treatment group to the mean absorbance for the control group. MTT assays of cells incubated in the medium without polymers were set as the control.

$$\text{Cell viability (\%)} = \frac{\overline{\text{Abs}}_{\text{Treatment group}}}{\overline{\text{Abs}}_{\text{Control group}}} \times 100.$$

The statistical analysis was compared using Student's *t*-test over five nominally identical measurements. The results were expressed as the mean ± SD% and considered to be statistically significant when $p < 0.05$.

Flow cytometry

Bel-7402 cells were plated in a 6-well plate at a density of 1×10^6 per well and grown overnight in 5% CO_2 at 37 °C. Then the polymeric probes were added from a concentrated stock solution in PBS at a final concentration of 0.025 mg mL^{-1} and incubated for 1 h. After discarding the media and rinsing three times with PBS, the cells were harvested by trypsinization. After centrifugation, the cell pellets were washed carefully with PBS, re-suspended in PBS and analyzed immediately using a BD FACSAria flow cytometer (BD Biosciences) operating at 488 nm excitation and with a 610/20 nm emission filter set. The cell suspension was illuminated for 30 s to convert the SP polymers to MC polymers using a 365 nm UV LED before flow cytometric analysis.

Cellular imaging

The cells were seeded at a density of 1×10^5 per well on each 35 mm glass bottom culture dish (NEST Biotechnology Co., Ltd), and incubated overnight in 5% CO_2 at 37 °C. Then the polymeric probes were added from a concentrated stock solution in PBS at a final concentration of 0.025 mg mL^{-1} and incubated for 1 h. After discarding the media and rinsing three times with PBS, cultured cells were placed in fresh warm serum-free growth medium. Cell imaging was performed with an OLYMPUS ZX81 confocal laser scanning microscope equipped with a 63× oil-immersion objective lens and a Leica TCS SP5 MP confocal laser scanning microscope equipped with a 63× oil-immersion objective lens, a temperature control module, an argon ion laser and a Coherent Chameleon Ti:sapphire laser as the two-photon excitation source, which could be tuned over the range of 720–950 nm. For the single-photon excitation fluorescence imaging, cells were excited at 488 nm and emissions were collected using a 630/30 nm filter set. For the two-photon excitation fluorescence imaging, cells were illuminated using the NIR laser (750 nm) and single-photon laser (488 nm) alternately to intensify and erase the red fluorescence signals, respectively.

Results and discussion

The norbornenyl monomer NB–Boc–NH was obtained *via* the typical condensation reaction between *exo*-norbornenyl carboxylic acid[70–72] and *N*-(*tert*-butoxycarbonyl)hexyl diamine[73] in the presence of PyBOP and TEA in DMF, with an excellent yield of 91%. The spiropyran monomer NB–SP and hydrophilic monomer NB–P3 were synthesized according to our previous report.[58] For the preparation of our designed copolymers, the living character of the polymerization for the NB–Boc–NH and NB–P3 monomers was firstly investigated. Both were subject to ROMP individually using Grubbs' third-generation initiator at room temperature in degassed methylene chloride. Fig. 1 shows the molecular weights (M_n) of these homopolymers *versus* the monomer to initiator ratios (Fig. S1 and Table S1, ESI†). Four different polymerizations were carried out with monomer to initiator ratios of 25 : 1, 50 : 1, 75 : 1 and 100 : 1. A linear plot suggests a high degree of control over the polymerization. Moreover, the ^{1}H NMR spectra (Fig. S2†) show complete disappearance of the carbene signal of the initiator at 19.1 ppm, and at the same time the formation of two new broad carbene

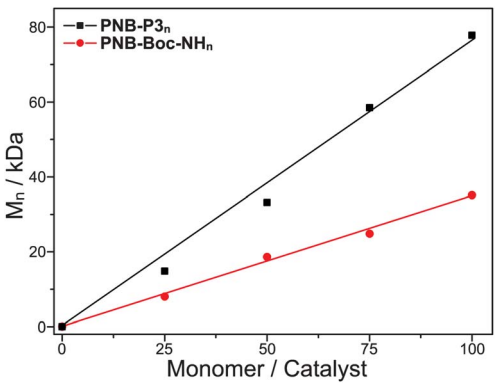

Fig. 1 Plot of M_n *vs.* the monomer to initiator ratios for the ROMP of NB–Boc–NH and NB–P3 monomers.

Table 1 GPC and zeta potential data for the PNB–SP_x-*co*-(Boc–NH)$_y$-*co*-P3$_z$ and PNB–SP_x-*co*-(NH_2·HCl)$_y$-*co*-P3$_z$ water-soluble random copolymers

Polymer[a]	M_n/kDa	M_w/kDa	PDI	ζ potential[b]/mV
PNB–SP_{20}-*co*-P3$_{80}$	77.2	93.8	1.22	−2.43
PNB–SP_{20}-*co*-(Boc–NH)$_{10}$-*co*-P3$_{70}$	70.5	88.7	1.26	—
PNB–SP_{20}-*co*-(Boc–NH)$_{20}$-*co*-P3$_{60}$	60.4	76.8	1.27	—
PNB–SP_{20}-*co*-(Boc–NH)$_{30}$-*co*-P3$_{50}$	60.3	81.5	1.35	—
PNB–SP_{20}-*co*-(NH_2·HCl)$_{10}$-*co*-P3$_{70}$	60.2	76.9	1.28	+13.2
PNB–SP_{20}-*co*-(NH_2·HCl)$_{20}$-*co*-P3$_{60}$	44.1	56.4	1.28	+13.7
PNB–SP_{20}-*co*-(NH_2·HCl)$_{30}$-*co*-P3$_{50}$	43.2	58.1	1.34	+15.6

[a] Measured in DMF with 10 mM LiBr at 313 K. [b] Measured in 10 mM PBS buffer (pH 7.4) with the concentration of 1.0 mg mL^{-1} at 298 K.

signals at 18.7 and 18.4 ppm. These observations clearly demonstrate a living fashion of ROMP for the Boc-protected amino monomer NB–Boc–NH and the hydrophilic monomer NB–P3.[45,46]

Based on our previous study, water-soluble PNB–SP_x-*co*-(Boc–NH)$_y$-*co*-P3$_z$ copolymers were prepared empirically from suitable feeding proportions of the photochromic spiropyran monomer NB–SP, amino monomer NB–Boc–NH and hydrophilic monomer NB–P3. As the degree of polymerization (DP) was fixed at 100, *i.e.* the molar ratio of the total feeding amounts of the monomers to Grubbs' third-generation initiator was 100 : 1, the spiropyran monomer proportion x was chosen as 20 and the NB–Boc–NH monomer proportion y was varied from 0 to 30. The GPC data is listed in Table 1. The PDIs of the resulting PNB–SP_x-*co*-(Boc–NH)$_y$-*co*-P3$_z$ copolymers were relatively narrow, ranging from 1.22 to 1.35, and the molecular weight M_n was in the range of 60–77 kDa, which showed a reasonable relationship with the total feeding amounts of the monomers.

For the activation of the Boc-protected amino group, the PNB–SP_x-*co*-(Boc–NH)$_y$-*co*-P3$_z$ copolymers were deprotected by a standard treatment with a mixture of 95% TFA, 2.5% H_2O and 2.5% triisopropylsilane. Here, triisopropylsilane served as a radical scavenger for stabilizing the deprotected amino group. After counterion exchange with NaCl and dialysis in a refrigerator, the activated PNB–SP_x-*co*-(NH_2·HCl)$_y$-*co*-P3$_z$ copolymers were obtained as yellow solids. The GPC measurements provided clear evidence for the decrease of the molecular weights (Fig. 2), while the corresponding retention volumes were obviously greater than those before the Boc-deprotection.

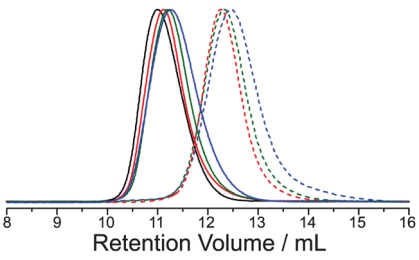

Fig. 2 Normalized GPC curves of the PNB–SP_x-*co*-(Boc–NH)$_y$-*co*-P3$_z$ (solid line) and PNB–SP_x-*co*-(NH_2·HCl)$_y$-*co*-P3$_z$ (dashed line) copolymers: $x = 20$, $y = 0$, $z = 80$ (black); $x = 20$, $y = 10$, $z = 70$ (red); $x = 20$, $y = 20$, $z = 60$ (green); $x = 20$, $y = 30$, $z = 50$ (blue).

The chemical structure for copolymers and their components were investigated by FT-IR (Fig. 3). The spiropyran homopolymer PNB–SP (Fig. 3c, blue) exhibited an almost identical spectrum as its monomer NB–SP,[75] presenting typical NO_2 asymmetric and symmetric stretching vibrations at 1512 and 1337 cm^{-1}, alkyl-N stretching at 1297 cm^{-1}, phenyl-N stretching at 1275 cm^{-1}, O–C–N stretching at 955 cm^{-1}, and aromatic C–H out-of-plane deformation at 810 and 750 cm^{-1}. Besides, the vibration peak at 3062 cm^{-1} is attributed to alkene C–H stretching on the polynorbornene backbone or aromatic C–H. Other vibration peaks were observed at 1725, 1170 and 1091 cm^{-1} for C=O, alkyl-O and phenyl-O stretching, respectively. The hydrophilic homopolymer PNB–P3 (Fig. 3e, purple) showed strong vibration peaks attributed to alkyl C–H stretching at 2800–3000 cm^{-1}, C=O stretching at 1728 cm^{-1}, alkyl-O stretching at 1199 cm^{-1} and phenyl-O stretching at 1112 cm^{-1}, which should be assigned to the repeated oligo-ethylene glycol units. Bearing the Boc-protected amino group, the PNB–Boc–NH homopolymer exhibited strong N–H stretching and bending peaks at 3332 and 1646 cm^{-1}, respectively (Fig. 3d, green), and the carbonyl stretching vibration of the amide linkage shifted to 1689 cm^{-1}, which has an obvious difference to that of the ester. The FT-IR spectrum for the PNB–SP_{20}-*co*-(Boc–NH)$_{20}$-*co*-P3$_{60}$

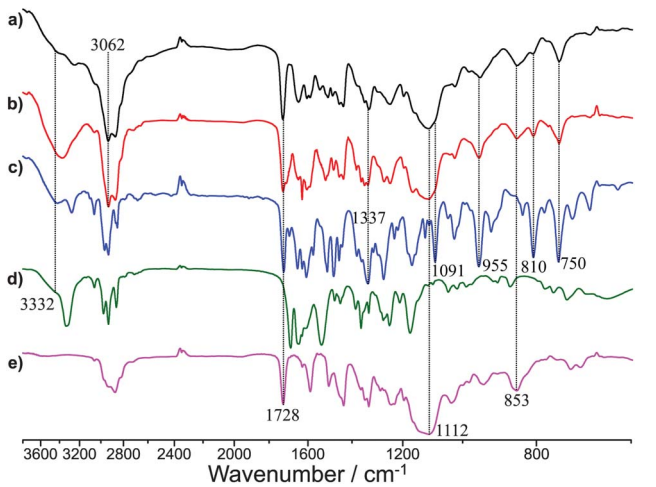

Fig. 3 FT-IR spectra of the deprotected PNB–SP_{20}-*co*-(NH_2·HCl)$_{20}$-*co*-P3$_{60}$ (a, black), PNB–SP_{20}-*co*-(Boc–NH)$_{20}$-*co*-P3$_{60}$ (b, red), PNB–SP (c, blue), NB–Boc–NH (d, green) and PNB–P3 (e, purple) polymers.

copolymer was well represented as a composite of the above three components (Fig. 3b, red). After standard treatment with TFA, the vibration peaks for N–H stretching at 3369 cm^{-1}, C=O stretching at 1729 cm^{-1} and N–H bending at 1650 cm^{-1} were greatly decreased in the activated PNB–SP_{20}-*co*-$(NH_2 \cdot HCl)_{20}$-*co*-$P3_{60}$ copolymer (Fig. 3a, black), suggesting the removal of the Boc pretecting group.

The similarity in chemical structure for the activated and Boc-protected copolymers was also corroborated by ^1H NMR, shown in Fig. 4. The spectrum of the PNB–SP_{20}-*co*-$(Boc–NH)_{20}$-*co*-$P3_{60}$ copolymer resembles a stoichiometric superposition of its PNB–SP, PNB–Boc–NH and PNB–P3 homopolymer components (see Fig. S22–24, ESI† for details). A single peak at 1.43 ppm clearly indicates the existence of the tertiary butyl group in the Boc-protected copolymer. After deprotection this signal peak disappears, suggesting the formation of an ammonium group in the activated PNB–SP_{20}-*co*-$(NH_2 \cdot HCl)_{20}$-*co*-$P3_{60}$ copolymer.

Consistently, both the activated PNB–SP_{20}-*co*-$(NH_2 \cdot HCl)_{20}$-*co*-$P3_{60}$ and Boc-protected PNB–SP_{20}-*co*-$(Boc–NH)_{20}$-*co*-$P3_{60}$ copolymers exhibit excellent photochromism in aqueous media. Reversible photoisomerization of the SP units was clearly evidenced by UV-Vis absorption spectra, shown in Fig. 5 (see also Fig. S3, ESI†). On irradiating the aqueous solution of PNB–SP_{20}-*co*-$(NH_2 \cdot HCl)_{20}$-*co*-$P3_{60}$ by 365 nm UV light for 6 seconds, the photostationary states were reached. A strong absorption peak at 559 nm, characteristic of the MC isomer, appeared (Fig. S3, ESI,† top), and the colorless solution became deep blue. On irradiating the blue solution with 530 nm visible light, the MC unit isomerized back to the SP isomer in 200 s, and the absorption spectrum almost reverted to the original spectrum (Fig. S3, ESI,† bottom). No Stokes shifts were observed, which implies no aggregation or environmental changes to the SP or MC isomers during photoisomerization. The MC fluorescence of PNB–SP_{20}-*co*-$(NH_2 \cdot HCl)_{20}$-*co*-$P3_{60}$ was given as the red curve in Fig. 5 with a maximum emission peak at 638 nm and a lifetime of 2.87 ns (Fig. S4, ESI†). It shows no obvious difference from that of PNB–SP_{20}-*co*-$(Boc–NH)_{20}$–*co*-$P3_{60}$, with a maximum emission peak at 636 nm and a lifetime of 1.73 ns (Fig. S5, ESI†).

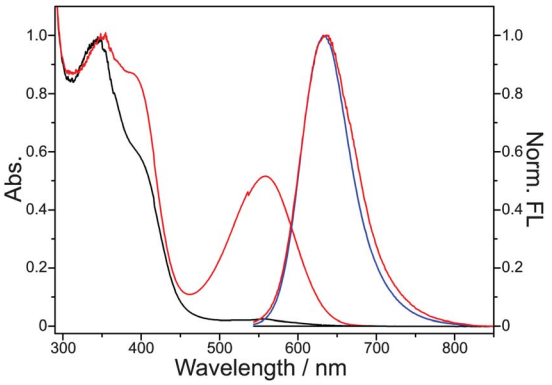

Fig. 5 UV-Vis absorption and normalized fluorescence spectra of the non-fluorescent SP form (black) and fluorescent MC form (red) of PNB–SP_{20}-*co*-$(NH_2 \cdot HCl)_{20}$-*co*-$P3_{60}$ with a concentration of 0.082 mg mL^{-1}; and the normalized fluorescence spectrum of deprotected PNB–SP_{20}-*co*-$(NH_2 \cdot HCl)_{20}$-*co*-$P3_{60}$ (blue) with a concentration of 0.087 mg mL^{-1} in 10 mM PBS buffer.

Cytotoxicity is essential for the application of polynorbornenes in fluorescence imaging. Here, the effect of PNB–SP_{20}-*co*-$(NH_2 \cdot HCl)_{20}$-*co*-$P3_{60}$ on the proliferation of Bel-7402, HepG2, MCF-7 and A549 cells was accessed using a modified MTT assay. When the concentration of the polymer is lower than 0.10 mg mL^{-1}, the cell viabilities are greater than 96%; when the concentration of the polymer is as high as 0.20 mg mL^{-1} the cell viabilities remain at 91%, as shown in Fig. 6. This observation suggests that the cytotoxicity of the polynorbornenes is very low and may benefit the single- and two-photon *in vitro* fluorescence imaging.

Cell transporting capability is also essential for the application of polynorbornenes in fluorescence imaging. The activated ammonium group can significantly enhance the cell uptake efficiency of these multi-component polymers. The fluorescence

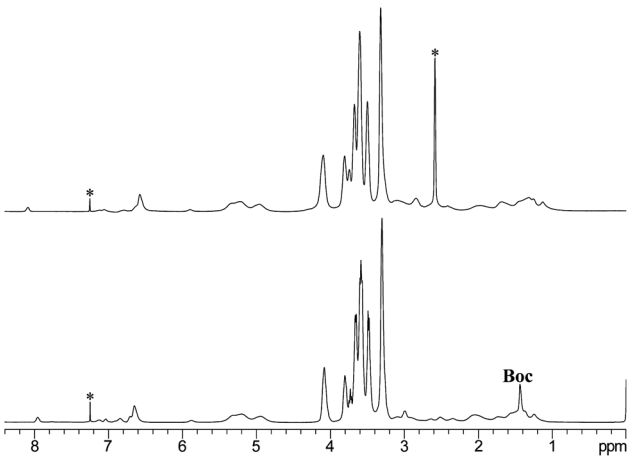

Fig. 4 ^1H NMR spectra for PNB–SP_{20}-*co*-$(Boc–NH)_{20}$–*co*-$P3_{60}$ (bottom) in $CDCl_3$ and deprotected PNB–SP_{20}-*co*-$(NH_2 \cdot HCl)_{20}$-*co*-$P3_{60}$ (top) in DMSO-d_6/$CDCl_3$ (v/v, 3 : 1). The residual solvents are marked with stars.

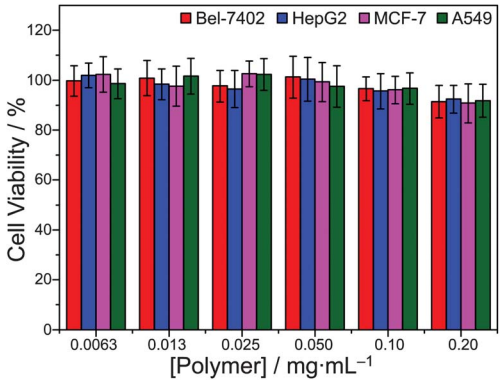

Fig. 6 Metabolic viability of Bel-7402 (red), HepG2 (blue), MCF-7 (purple) and A549 (green) cells after incubation with the PNB–SP_{20}-*co*-$(NH_2 \cdot HCl)_{20}$-*co*-$P3_{60}$ copolymer at various concentrations for 24 h.

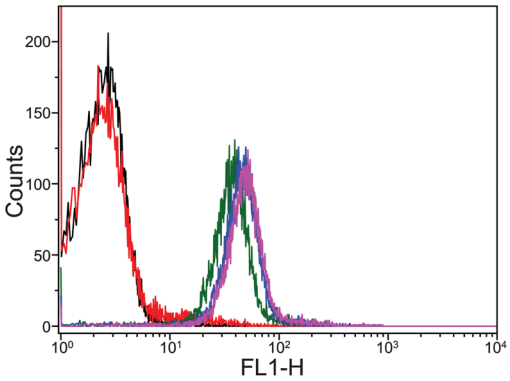

Fig. 7 Flow cytometry histograms of the Bel-7402 cells after 1 h incubation with 0.025 mg mL^{-1} PNB–SP_x-*co*-$(NH_2 \cdot HCl)_y$-*co*-$P3_z$ copolymers: control experiment (black), $x = 20$, $y = 0$, $z = 80$ (red); $x = 20$, $y = 10$, $z = 70$ (green); $x = 20$, $y = 20$, $z = 60$ (blue); $x = 20$, $y = 30$, $z = 50$ (purple), illuminated with a 365 nm UV LED for 30 s.

profiles of the PNB–SP_x-*co*-$(NH_2 \cdot HCl)_y$-*co*-$P3_z$ copolymers was quantitatively studied by flow cytometry in Bel-7402 cells, and the histograms are shown as Fig. 7. With more cationic ammonium groups on the polynorbornene backbones, the cell uptake of the PNB–SP_x-*co*-$(NH_2 \cdot HCl)_y$-*co*-$P3_z$ copolymers is more efficient, which is in agreement with the increasing of the positive ζ potentials listed in Table 1. In the absence of activated ammonium groups, the neutral PNB–SP_{20}-*co*-$P3_{80}$ copolymer with a ζ potential of −2.43 mV exhibits no cell transporting capability. Since cell membranes are weakly negatively charged, electrostatic interactions drive the cationic PNB–SP_x-*co*-$(NH_2 \cdot HCl)_y$-*co*-$P3_z$ polynorbornenes to easily anchor to cell membranes and internalize into cells through a charge-mediated endocytosis process.[69] In addition, the control experiment at 4 °C (Fig. S7, ESI†) suggests that the internalization of PNB–SP_{20}-*co*-$(NH_2 \cdot HCl)_{20}$-*co*-$P3_{60}$ is dramatically inhibited at low temperature, which indicates that the uptake of polynorbornenes by Bel-7402 cells is through an energy-dependent pathway.[32]

The application of multi-component polynorbornenes for cellular fluorescence imaging was investigated by confocal laser scanning microscopy. Bearing a photo-responsive SP component, the PNB–SP_{20}-*co*-$(NH_2 \cdot HCl)_{20}$-*co*-$P3_{60}$ copolymer exhibits switchable fluorescence imaging characteristics with alternating NIR two-photon and visible single-photon excitations in Bel-7402, HepG2, MCF-7 and A549 cells, as shown in Fig. 8. A cycle of optical switching begins with excitation of the non-fluorescent SP form within a single scan with a 750 nm NIR laser, eliciting an excited-state isomerization to the fluorescent MC form. Subsequent excitation of MC using a 488 nm visible laser induces either red fluorescence or gradual photoisomerization back to the non-fluorescent SP form. Such switching cycles regulated by NIR and visible laser illumination could be repeated for more than ten cycles in Bel-7402 cells (Fig. 9), as well as in HepG2, MCF-7 and A549 cells (Fig. S9–11 in ESI†). The fluorescent signal from the cytoplasm is observed clearly to distinguish the cell

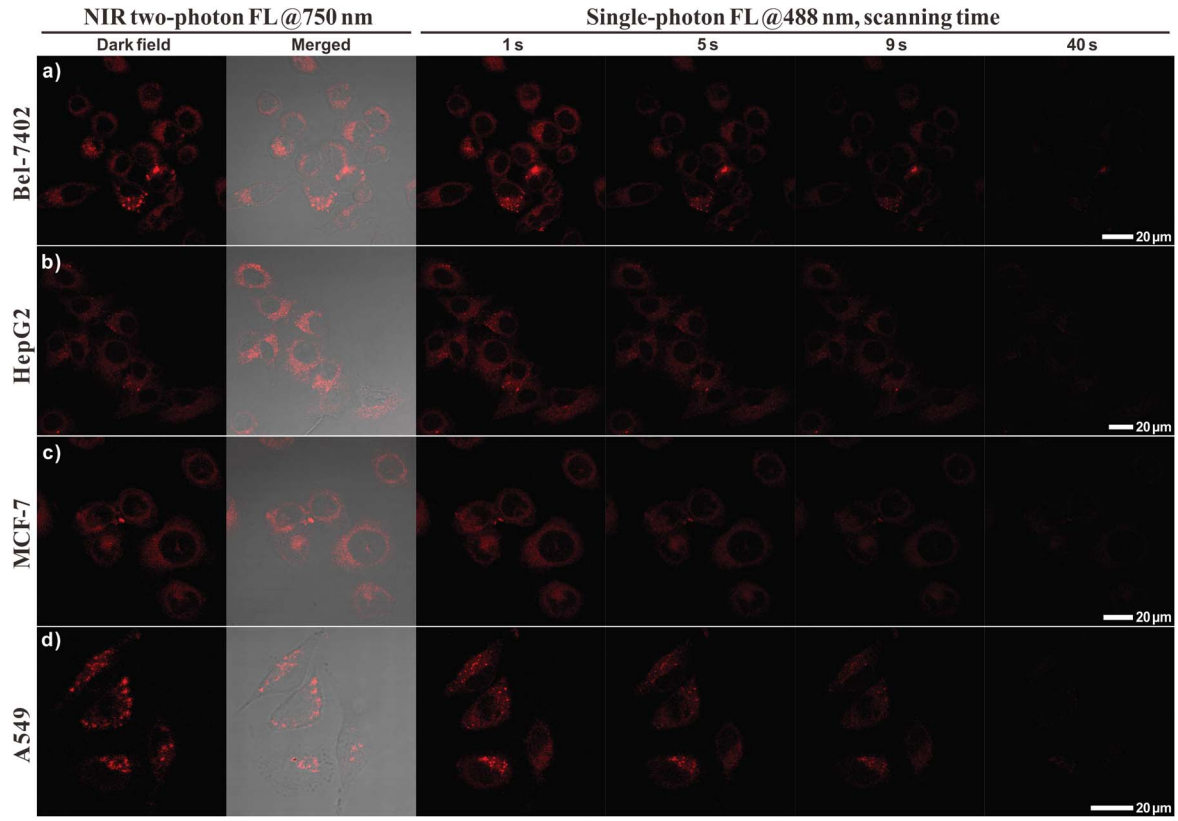

Fig. 8 NIR two-photon fluorescence imaging and time-dependent single-photon fluorescence decay for Bel-7402 (a), HepG2 (b), MCF-7 (c) and A549 (d) cells.

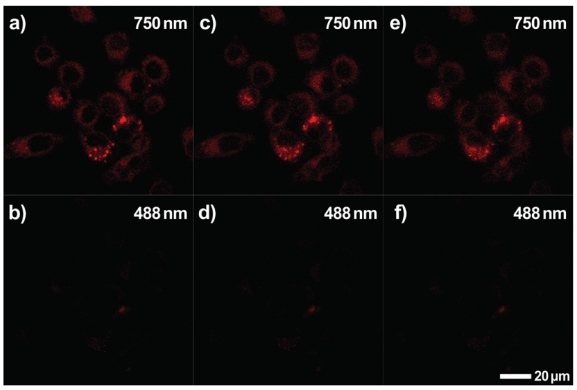

Fig. 9 The switching of fluorescence imaging with alternating NIR two-photon (a, c and e) and visible single-photon (b, d and f) excitations for Bel-7402 cells.

profile, demonstrating that multi-component PNB–SP_x-*co*-$(NH_2 \cdot HCl)_y$-*co*-$P3_z$ polynorbornenes can serve as promising switchable NIR two-photon fluorescent probes.

Conclusions

In summary, a set of water-soluble new copolymers were achieved *via* a one-pot multi-component ROMP from hydrophilic norbornenes. Due to containing a photochromic spiropyran component, these polynorbornenes exhibit switchable fluorescence imaging characteristics when receiving NIR two-photon and visible single-photon excitations in cancer cells, and are promising NIR two-photon fluorescent imaging agents. By introducing a cationic ammonium group, the cell transporting capability of the imaging polynorbornenes could be significantly enhanced. Moreover, the strategy of one-pot ROMP makes polynorbornene a modular and flexible scaffold for the design and synthesis of specifically biocompatible polymers for multipurpose applications in imaging, diagnosis and therapy.

Acknowledgements

This work was finished in Beijing Area Major Laboratory of Peptide and Small Molecular Drugs and supported by the Ministry of Science and Technology of China (2013CB834505 and 2014CB239402), the National Natural Science Foundation of China (21204052, 21002108, 21372232 and 91027041), Beijing Municipal Education Commission Science & Technology (KM201110025003), Solar Energy Initiative of the Knowledge Innovation Program of CAS, the Bureau for Basic Research of CAS, and the Foundation of Director of Technical Institute of Physics and Chemistry, CAS.

Notes and references

1 W. J. M. Mulder, G. J. Strijkers, G. A. F. van Tilborg, D. P. Cormode, Z. A. Fayad and K. Nicolay, *Acc. Chem. Res.*, 2009, **42**, 904–914.
2 H. Kobayashi, M. R. Longmire, M. Ogawa and P. L. Choyke, *Chem. Soc. Rev.*, 2011, **40**, 4626–4648.
3 A. Louie, *Chem. Rev.*, 2010, **110**, 3146–3195.
4 C. Zhu, L. Liu, Q. Yang, F. Lv and S. Wang, *Chem. Rev.*, 2012, **112**, 4687–4735.
5 T. Xia, N. Li and X. Fang, *Annu. Rev. Phys. Chem.*, 2013, **64**, 459–480.
6 J. Zhang, R. E. Campbell, A. Y. Ting and R. Y. Tsien, *Nat. Rev. Mol. Cell Biol.*, 2002, **3**, 906–918.
7 Y. Zou, T. Yi, S. Xiao, F. Li, C. Li, X. Gao, J. Wu, M. Yu and C. Huang, *J. Am. Chem. Soc.*, 2008, **130**, 15750–15751.
8 W. Tan, J. Zhou, F. Li, T. Yi and H. Tian, *Chem.–Asian J.*, 2011, **6**, 1263–1268.
9 D.-E. Lee, H. Koo, I.-C. Sun, J. H. Ryu, K. Kim and I. C. Kwon, *Chem. Soc. Rev.*, 2012, **41**, 2656–2672.
10 X. Michalet, F. F. Pinaud, L. A. Bentolila, J. M. Tsay, S. Doose, J. J. Li, G. Sundaresan, A. M. Wu, S. S. Gambhir and S. Weiss, *Science*, 2005, **307**, 538–544.
11 N. Li, C. Chang, W. Pan and B. Tang, *Angew. Chem., Int. Ed.*, 2012, **51**, 7426–7430.
12 S.-H. Cheng, F.-C. Li, J. S. Souris, C.-S. Yang, F.-G. Tseng, H.-S. Lee, C.-T. Chen, C.-Y. Dong and L.-W. Lo, *ACS Nano*, 2012, **6**, 4122–4131.
13 H.-C. Huang, S. Barua, G. Sharma, S. K. Dey and K. Rege, *J. Controlled Release*, 2011, **155**, 344–357.
14 J. Zhou, Z. Liu and F. Li, *Chem. Soc. Rev.*, 2012, **41**, 1323–1349.
15 Y. He, H. Lu, Y. Su, L. Sai, M. Hu, C. Fan and L. Wang, *Biomaterials*, 2011, **32**, 2133–2140.
16 C. Peng, W. Hu, Y. Zhou, C. Fan and Q. Huang, *Small*, 2010, **6**, 1686–1692.
17 A. M. Nyström and K. L. Wooley, *Acc. Chem. Res.*, 2011, **44**, 969–978.
18 K.-Y. Pu and B. Liu, *Adv. Funct. Mater.*, 2011, **21**, 3408–3423.
19 Z. Ge and S. Liu, *Chem. Soc. Rev.*, 2013, **42**, 7289–7325.
20 N. Kamaly, Z. Xiao, P. M. Valencia, A. F. Radovic-Moreno and O. C. Farokhzad, *Chem. Soc. Rev.*, 2012, **41**, 2971–3010.
21 U. Boas and P. M. H. Heegaard, *Chem. Soc. Rev.*, 2004, **33**, 43–63.
22 D. F. Baban and L. W. Seymour, *Adv. Drug DeliveryRev.*, 1998, **34**, 109–119.
23 H. Maeda, J. Wu, T. Sawa, Y. Matsumura and K. Hori, *J. Controlled Release*, 2000, **65**, 271–284.
24 A. K. Iyer, G. Khaled, J. Fang and H. Maeda, *Drug Discovery Today*, 2006, **11**, 812–818.
25 T. Liu, J. Hu, Z. Jin, F. Jin and S. Liu, *Adv. Healthcare Mater.*, 2013, DOI: 10.1002/adhm.201200436.
26 J. Hu, T. Liu, G. Zhang, F. Jin and S. Liu, *Macromol. Rapid Commun.*, 2012, 749–758.
27 D. Ding, G. Wang, J. Liu, K. Li, K.-Y. Pu, Y. Hu, J. C. Y. Ng, B. Z. Tang and B. Liu, *Small*, 2012, **8**, 3523–3530.
28 X. Feng, Y. Tang, X. Duan, L. Liu and S. Wang, *J. Mater. Chem.*, 2010, **20**, 1312–1316.
29 G. Feng, D. Ding and B. Liu, *Nanoscale*, 2012, **4**, 6150–6165.
30 E. N. Savariar, S. V. Aathimanikandan and S. Thayumanavan, *J. Am. Chem. Soc.*, 2006, **128**, 16224–16230.

31 Z. Hordyjewicz-Baran, L. You, B. Smarsly, R. Sigel and H. Schlaad, *Macromolecules*, 2007, **40**, 3901–3903.
32 H. Lu, F. Su, Q. Mei, Y. Tian, W. Tian, R. H. Johnson and D. R. Meldrum, *J. Mater. Chem.*, 2012, **22**, 9890–9900.
33 A. Fürstner, *Angew. Chem., Int. Ed.*, 2000, **39**, 3012–3043.
34 T. M. Trnka and R. H. Grubbs, *Acc. Chem. Res.*, 2000, **34**, 18–29.
35 *Olefin Metathesis and Metathesis Polymerization*, ed. J. M. Ivin and I. C. Mol, Academic, New York, 2nd edn, 1996.
36 R. H. Grubbs, *Handbook of Metathesis*, Wiley-VCH, Weinheim, Germany, 2003.
37 J. A. Love, J. P. Morgan, T. M. Trnka and R. H. Grubbs, *Angew. Chem., Int. Ed.*, 2002, **41**, 4035–4037.
38 K. Vehlow, D. Wang, M. R. Buchmeiser and S. Blechert, *Angew. Chem., Int. Ed.*, 2008, **47**, 2615–2618.
39 M. Lichtenheldt, D. Wang, K. Vehlow, I. Reinhardt, C. Kühnel, U. Decker, S. Blechert and M. R. Buchmeiser, *Chem.–Eur. J.*, 2009, **15**, 9451–9457.
40 U. Drechsler, R. J. Thibault and V. M. Rotello, *Macromolecules*, 2002, **35**, 9621–9623.
41 E. J. Foster, E. B. Berda and E. W. Meijer, *J. Am. Chem. Soc.*, 2009, **131**, 6964–6966.
42 E. B. Berda, E. J. Foster and E. W. Meijer, *Macromolecules*, 2010, **43**, 1430–1437.
43 Y. Xia, B. D. Olsen, J. A. Kornfield and R. H. Grubbs, *J. Am. Chem. Soc.*, 2009, **131**, 18525–18532.
44 Y. Xia, J. A. Kornfield and R. H. Grubbs, *Macromolecules*, 2009, **42**, 3761–3766.
45 K. Lienkamp, A. E. Madkour, A. Musante, C. F. Nelson, K. Nüsslein and G. N. Tew, *J. Am. Chem. Soc.*, 2008, **130**, 9836–9843.
46 G. J. Gabriel, A. E. Madkour, J. M. Dabkowski, C. F. Nelson, K. Nüsslein and G. N. Tew, *Biomacromolecules*, 2008, **9**, 2980–2983.
47 J. M. Pollino, L. P. Stubbs and M. Weck, *Macromolecules*, 2003, **36**, 2230–2234.
48 C. R. South, C. Burd and M. Weck, *Acc. Chem. Res.*, 2006, **40**, 63–74.
49 S. K. Yang, A. V. Ambade and M. Weck, *Chem. Soc. Rev.*, 2011, **40**, 129–137.
50 K. S. Roberts and N. S. Sampson, *J. Org. Chem.*, 2003, **68**, 2020–2023.
51 D. Le, V. Montembault, J. C. Soutif, M. Rutnakornpituk and L. Fontaine, *Macromolecules*, 2010, **43**, 5611–5617.
52 S. Sutthasupa, M. Shiotsuki, H. Matsuoka, T. Masuda and F. Sanda, *Macromolecules*, 2010, **43**, 1815–1822.
53 N. B. Sankaran, A. Z. Rys, R. Nassif, M. K. Nayak, K. Metera, B. Chen, H. S. Bazzi and H. F. Sleiman, *Macromolecules*, 2010, **43**, 5530–5537.
54 S. C. G. Biagini and A. L. Parry, *J. Polym. Sci., Part A: Polym. Chem.*, 2007, **45**, 3178–3190.
55 K. Miki, Y. Kuramochi, K. Oride, S. Inoue, H. Harada, M. Hiraoka and K. Ohe, *Bioconjugate Chem.*, 2009, **20**, 511–517.
56 F. Gueugnon, I. Denis, D. Pouliquen, F. Collette, R. Delatouche, V. Héroguez, M. Grégoire, P. Bertrand and C. Blanquart, *Biomacromolecules*, 2013, **14**, 2396–2402.
57 Y. Zhang, Q. Yin, H. Lu, H. Xia, Y. Lin and J. Cheng, *ACS Macro Lett.*, 2013, **2**, 809–813.
58 K. Feng, N. Xie, B. Chen, L.-P. Zhang, C.-H. Tung and L.-Z. Wu, *Macromolecules*, 2012, **45**, 5596–5603.
59 Y. Zhao, *Macromolecules*, 2012, **45**, 3647–3657.
60 P. Gorostiza and E. Y. Isacoff, *Science*, 2008, **322**, 395–399.
61 G. Marriott, S. Mao, T. Sakata, J. Ran, D. K. Jackson, C. Petchprayoon, T. J. Gomez, E. Warp, O. Tulyathan, H. L. Aaron, E. Y. Isacoff and Y. Yan, *Proc. Natl. Acad. Sci. U. S. A.*, 2008, **105**, 17789–17794.
62 M.-Q. Zhu, G.-F. Zhang, C. Li, M. P. Aldred, E. Chang, R. A. Drezek and A. D. Q. Li, *J. Am. Chem. Soc.*, 2010, **133**, 365–372.
63 G. S. He, L.-S. Tan, Q. Zheng and P. N. Prasad, *Chem. Rev.*, 2008, **108**, 1245–1330.
64 W. Denk, J. Strickler and W. Webb, *Science*, 1990, **248**, 73–76.
65 W. R. Zipfel, R. M. Williams and W. W. Webb, *Nat. Biotechnol.*, 2003, **21**, 1369–1377.
66 F. Helmchen and W. Denk, *Nat. Methods*, 2005, **2**, 932–940.
67 H. M. Kim and B. R. Cho, *Acc. Chem. Res.*, 2009, **42**, 863–872.
68 K. Li, Y. Jiang, D. Ding, X. Zhang, Y. Liu, J. Hua, S.-S. Feng and B. Liu, *Chem. Commun.*, 2011, **47**, 7323–7325.
69 R. I. Zhdanov, O. V. Podobed and V. V. Vlassov, *Bioelectrochemistry*, 2002, **58**, 53–64.
70 D. D. Manning, L. E. Strong, X. Hu, P. J. Beck and L. L. Kiessling, *Tetrahedron*, 1997, **53**, 11937–11952.
71 J. D. Roberts, E. R. Trumbull, W. Bennett and R. Armstrong, *J. Am. Chem. Soc.*, 1950, **72**, 3116–3124.
72 C. D. Ver Nooy and C. S. Rondestvedt, *J. Am. Chem. Soc.*, 1955, **77**, 3583–3586.
73 T. Kurtán, N. Nesnas, Y.-Q. Li, X. Huang, K. Nakanishi and N. Berova, *J. Am. Chem. Soc.*, 2001, **123**, 5962–5973.
74 F. M. Raymo and S. Giordani, *J. Am. Chem. Soc.*, 2001, **123**, 4651–4652.
75 K. H. Fries, J. D. Driskell, S. Samanta and J. Locklin, *Anal. Chem.*, 2010, **82**, 3306–3314.

